Journal of Biomedical Optics

BiomedicalOptics.SPIEDigitalLibrary.org

Polyethylene glycol molecular weight influences the Clear^{T2} optical clearing method for spheroids imaging by confocal laser scanning microscopy

Elisabete C. Costa
André F. Moreira
Duarte de Melo-Diogo
Ilídio J. Correia

SPIE.

Elisabete C. Costa, André F. Moreira, Duarte de Melo-Diogo, Ilídio J. Correia, "Polyethylene glycol molecular weight influences the Clear^{T2} optical clearing method for spheroids imaging by confocal laser scanning microscopy," *J. Biomed. Opt.* **23**(5), 055003 (2018), doi: 10.1117/1.JBO.23.5.055003.

Polyethylene glycol molecular weight influences the Clear^{T2} optical clearing method for spheroids imaging by confocal laser scanning microscopy

Elisabete C. Costa,[a] André F. Moreira,[a] Duarte de Melo-Diogo,[a] and Ilídio J. Correia[a,b,*]
[a]Universidade da Beira Interior, Centro de Investigação em Ciências da Saúde—Health Sciences Research Centre, Covilhã, Portugal
[b]Universidade de Coimbra, Centro de Investigação em Engenharia dos Processos Químicos e dos Produtos da Floresta—Departamento de Engenharia Química, Coimbra, Portugal

Abstract. Some fluorescence microscopy techniques, such as confocal laser scanning microscopy (CLSM), have a limited penetration depth. Consequently, the visualization and imaging of three-dimensional (3-D) cell cultures, such as spheroids, using these methods can be a significant challenge. Therefore, to improve the imaging of 3-D tissues, optical clearing methods have been optimized to render transparency to the opaque spheroids. The influence of the polyethylene glycol (PEG) molecular weight (MW) used in the Clear^{T2} method for the imaging of propidium iodide (PI)-stained spheroids was investigated. The results demonstrated that the Clear^{T2} clearing method contributes to spheroids transparency and to the preservation of PI fluorescence intensity for all the PEG MW used (4000, 8000, and 10,000 Da). Furthermore, the Clear^{T2} method performed using PEG 4000 Da allowed a better PI signal penetration depth and cross-section depth. Overall, the optimization of PEG MW can improve the imaging of intact spheroids by CLSM. Furthermore, this work may also contribute to increase the application of 3-D cell culture models by the pharmaceutical industry for the high-throughput screening of therapeutics. [DOI: 10.1117/1.JBO.23.5.055003]

Keywords: Clear^{T2}; confocal laser scanning microscopy; polyethylene glycol; propidium iodide; spheroids.

Paper 180066R received Feb. 3, 2018; accepted for publication Apr. 17, 2018; published online May 11, 2018.

1 Introduction

During the preclinical drug development phase, compound libraries must be thoroughly tested. For this purpose, cells cultured as monolayers on flat surfaces are the gold-standard model used to evaluate the effectiveness and safety of the therapeutics in development.[1] Still, this type of cell culture model has been associated with lack of correspondence between the results obtained *in vitro* and those obtained in *in vivo* or in clinical trials.[1–3] Therefore, there has been an increasing need to improve the reliability of the *in vitro* methodologies in the high-throughput screening of new drugs. To address this issue, three-dimensional (3-D) cell culture models have been developed. In the 1970s, 3-D cellular aggregates—spheroids—started to be produced with the aim of mimicking the features of solid tumors, such as cellular organization, cell–cell and cell–extracellular matrix (ECM) interactions, gene expression profile, and drug resistance mechanisms (reviewed in detail in Refs. 4 and 5).

Despite the advantages of 3-D cell cultures, performing experiments on spheroids introduces new challenges since the methodologies and the equipment currently used for therapeutics screening are only optimized for cells cultured as monolayers. Fluorescence microscopy, such as light-sheet-based fluorescence microscopy, two-photon microscopy, multiphoton microscopy, and single (or selective) plane illumination microscopy have demonstrated an excellent performance in the *in vitro* analysis of therapeutics on spheroids.[4,6,7] Still, most laboratories are equipped with confocal laser scanning microscopy (CLSM) apparatus, which has been used to determine spheroids' size,[8] morphology,[9] internal cellular organization,[10,11] and expression of proteins (e.g., α-tubulin and E-Cadherins),[10,12] as well as to evaluate the penetration and efficacy of therapeutics (e.g., drugs and delivery systems) in the spheroid.[8,13–15] However, taking into account that spheroids are thick opaque samples with diameters between few hundred micrometers and almost 1 mm, the observation of whole spheroids by CLSM is hindered by the low penetration depth of this equipment (usually <100 μm).[4,6,16] This handicap is usually surpassed by slicing the spheroids into thin sections (3 to 7 μm).[17,18] However, the sectioning of spheroids is a laborious and time-consuming process that depends on organic solvents and can induce the disruption of the initial morphology of the spheroid (due to the introduction of structural artifacts).[4,19,20]

Another approach that has been employed to facilitate the imaging of 3-D thick samples is the use of optical clearing methods. These clearing techniques have been applied in the deep imaging of embryos and mouse tissues (e.g., brain, skin, and skeletal muscle)[21–25] and more recently started to be applied in the imaging of spheroids.[26,27] In general, the optical clearing methods reduce the light scattering induced by the cells and make the samples more transparent, thus enhancing light penetration and, consequently, the images quality.[6]

The clearing methods developed so far include the 3DISCO, ACT-PRESTO, BABB, Clear^{T}, Clear^{T2}, CLARITY, CUBIC, FocusClear, FRUIT, iDISCO, PACT/PARS, RTF, Scale, Sca/

*Address all correspondence to: Ilídio J. Correia, E-mail: icorreia@ubi.pt

1083-3668/2018/$25.00 © 2018 SPIE

eA2, Sca/eS, Sca/eU2, SeeDB, SeeDB2, TDE, uDISCO, among others (reviewed by Azaripour et al.,[25] Tainaka et al.,[28] Richardson and Lichtman,[6] and Seo et al.[29]). In 2013, Clear^{T2} was described for the first time by Kuwajima et al.[22] Compared to the other methods, the Clear^{T2} is quicker, and it does not use detergents or organic solvents. The Clear^{T2} protocol involves the immersion of the samples in aqueous solutions with increasing concentrations of formamide and polyethylene glycol (PEG).[22] These clearing solutions will promote the replacement of the water inside the cells by the aqueous solutions of formamide and PEG until an equilibrium is reached, while maintaining the sample hydrated, reducing the overall refractive index (RI) of the sample and improving samples' transparency.[6,22,29,30] On the other side, PEG is used to maintain the integrity and stability of the fluorescently labeled elements (e.g., proteins) and, thus, avoids the fluorescence quenching prompted by the formamide.[6,22,29,30]

So far, PEG with a molecular weight (MW) of 8000 Da has been used in the Clear^{T2} method.[22,26] Still, some studies demonstrated that PEGs with other MW can also be used to stabilize proteins.[31,32] In this way, disclosing the optimal PEG MW for spheroids clearing by Clear^{T2} may improve their analysis through CLSM and their potential for high-throughput screening of therapeutics. Herein, the influence of the PEG MW (4000, 8000, and 10,000 Da) used in the Clear^{T2} method in the imaging of propidium iodide (PI)-stained spheroids was investigated. For this purpose, PI was selected since it is commonly applied for spheroids analysis,[10,33,34] and it was also used in other works, where clearing methods were investigated.[35–37] After imaging whole noncleared and cleared spheroids through optical and CLSM, images were analyzed to characterize the effect of the Clear^{T2} method variations on spheroids' morphology, transparency, fluorescence, imaging penetration depth, and cross-section imaging depth.

2 Materials and Methods

2.1 *Materials*

Normal human dermal fibroblasts (HFIB) were bought from PromoCell (Labclinics, S.A., Barcelona, Spain). Cell imaging plates were acquired from Ibidi GmbH (Ibidi, Munich, Germany). Agarose was purchased from Grisp (Porto, Portugal). Cell culture plates, T-flasks, and cell culture consumables were obtained from ThermoFisher Scientific (Porto, Portugal). Dulbecco's modified Eagle's medium F12 (DMEM-F12), formamide (≥99.5%), paraformaldehyde (PFA), phosphate-buffered saline (PBS), trypsin, ethylenediaminetetraacetate (EDTA), PEG 4000, 8000, and 10,000 Da were purchased from Sigma-Aldrich (Sintra, Portugal). Fetal bovine serum (FBS) was obtained from Biochrom AG (Berlin, Germany). PI was purchased from Invitrogen (Carlsbad, California).

2.2 *Methods*

2.2.1 *Cell line maintenance and HFIB spheroids production by micromolding*

HFIB were cultured in DMEM-F12, with 10% (v/v) FBS and 1% streptomycin and gentamycin, inside an incubator with a humidified atmosphere at 37°C and 5% CO_2.[10] After cells attained confluence, they were recovered using 0.25% trypsin (1:250) and EDTA 0.1% (w/v).

Spheroids were fabricated using agarose structures with spherical microwells to guide the cells self-assembly.[38] The agarose structures were produced by placing 2% (w/v) agarose solution on 3-D Petri Dish® templates (Microtissues Inc., Providence, Rhode Island).[13] Before use, the agarose structures were placed in 12-well cell culture plates and sterilized by UV radiation. HFIB cells were then seeded using 1×10^6 cells per agarose structure, prompting the formation of 81 spheroids. Spheroids were maintained in culture with DMEM-F12 [10% (v/v) FBS and 1% streptomycin and gentamycin] at 37°C in a humidified atmosphere with 5% CO_2.

2.2.2 *Whole HFIB spheroids fixation and staining with PI*

Spheroids used in the experiments grew for 6 days. After this period, whole spheroids were recovered and then subjected to a chemical fixation process that encompasses spheroids incubation with PFA 4% (w/v) during 24 h at 4°C.[10] The PFA solution was freshly prepared to minimize its autofluorescence.[39] After fixation, the spheroids were washed three times with PBS and then labeled with 1 mL of PI (10 μg/mL in H_2O), as previously described.[10,11] After 24 h of spheroids incubation with the fluorescent probe on a plate shaker at 100 rotations per minute (RPM), spheroids were washed three times with PBS to remove the excess of PI.

2.2.3 *Whole spheroids clearing using the* Clear^{T2} *method*

The Clear^{T2} clearing method variations (Clear^{T2}/4, Clear^{T2}/8, and Clear^{T2}/10 that use PEG with an MW of 4000, 8000, and 10,000 Da, respectively) were performed accordingly to previous works (see Fig. 1 for the pipeline overview of the method).[22,26]

Initially, whole PI-stained spheroids were immersed in a 25% formamide/10% PEG solution for 10 min. Afterward, spheroids were immersed in 50% formamide/20% PEG solution for 5 min

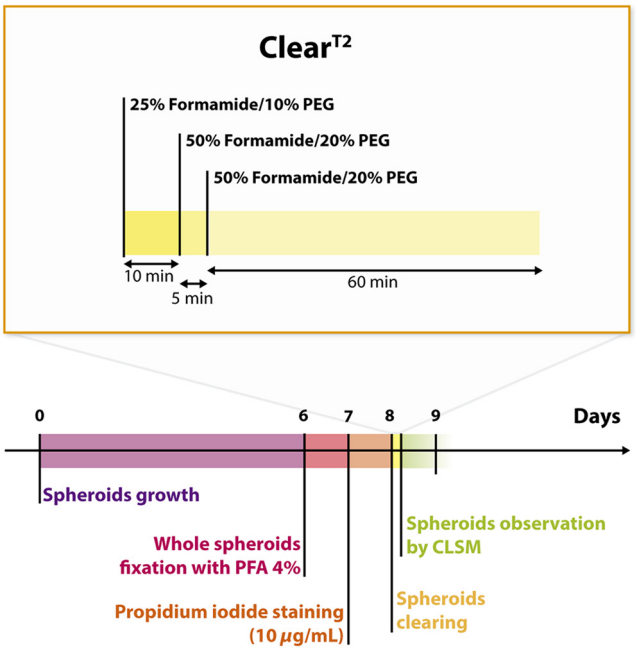

Fig. 1 Pipeline overview of the spheroids formation, labeling with the PI, and clearing with Clear^{T2}. The Clear^{T2} clearing procedure was performed using PEGs with different MWs: Clear^{T2}/4 (PEG 4000 Da), Clear^{T2}/8 (PEG 8000 Da), and Clear^{T2}/10 (PEG 10,000 Da).

and last in another 50% formamide/20% PEG solution for 1 h. PEG 4000, 8000, and 10,000 Da were used to prepare the solutions used in the Clear^{T2}/4, Clear^{T2}/8, and Clear^{T2}/10 method, respectively. All Clear^{T2} methods were performed at room temperature using a plate shaker at 100 RPM.

For comparative purposes, some spheroids were only immersed in PBS instead of the clearing solutions (noncleared PI-stained spheroids). Moreover, nonstained spheroids were subjected to Clear^{T2} methods (cleared nonstained spheroids) to evaluate the influence of the method in the spheroids' autofluorescence.

After the clearing of the intact spheroids, samples were transferred to μ-slide 8-well imaging plates (Ibidi GmbH, Germany) for imaging experiments.

2.2.4 *Whole spheroids imaging by optical and CLSM*

To observe any possible changes in spheroids size and transparency due to the clearing method, optical microscopy images were acquired using Olympus CX41 inverted optical microscope equipped with an Olympus SP-500 UZ digital camera and a Carl Zeiss Axio Imager A1 inverted microscope equipped with an AxioVision camera.

Images of intact HFIB spheroids were also acquired through CLSM using a Zeiss LSM 710 AxioObserver laser scanning confocal microscope (Carl Zeiss SMT, Inc., Oberkochen, Germany). For comparative purposes, all the samples were analyzed using the same equipment settings. The objective used was a 20× air objective (Plan-Apochromat 20 × /0.8 M27, working distance = 0.55 mm). The size of the confocal aperture was 1 Airy disk, and z-stacks were collected with 5-μm intervals. Laser power and master gain were kept constant during image acquisition. PI was visualized with a 514-nm argon laser.

After the acquisition of the CLSM images, an image analysis software—ImageJ, National Institutes of Health,[40] was used to determine PI fluorescence levels, imaging penetration depth, and cross-section imaging depth (see Figs. 6–8 in the Appendix for details). The results were compared and normalized to those obtained for noncleared PI-stained spheroids (spheroids that were only treated with PBS).

2.2.5 *Statistical analysis*

Data were expressed as mean value ± standard deviation (s.d.). The statistical analysis was performed using one-way analysis of variance test. A value of $p < 0.05$ was considered statistically significant. Data analysis was performed in GraphPad Prism v.6.0 software (trial version, GraphPad Software, California).

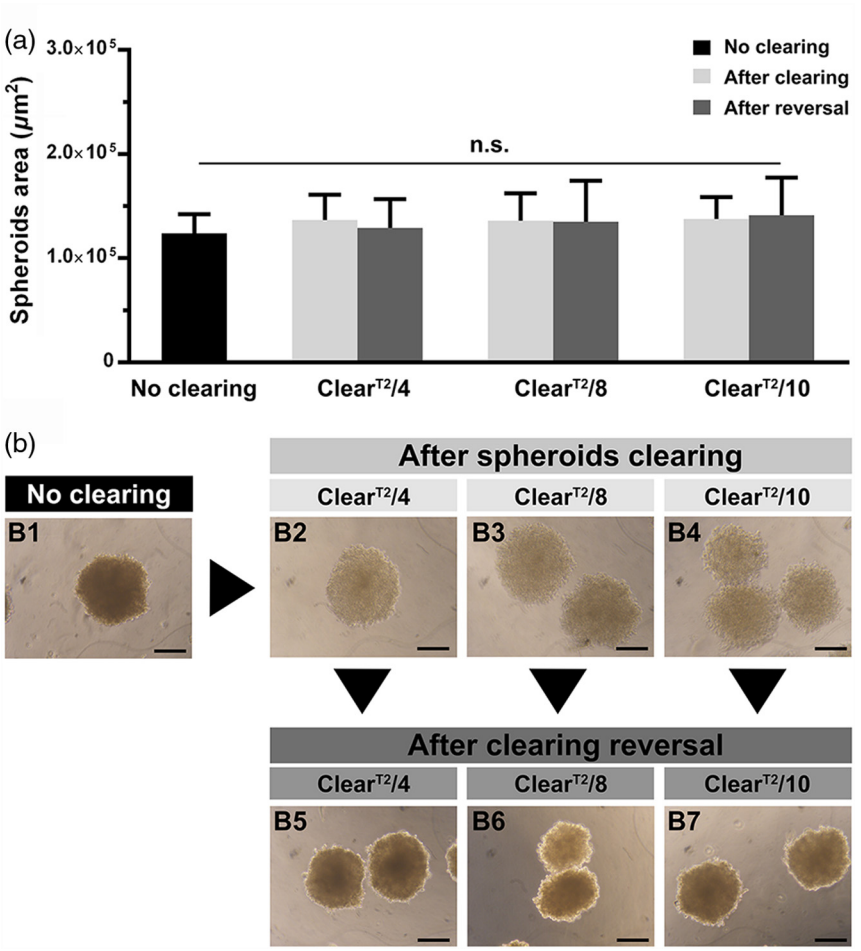

Fig. 2 Influence of Clear^{T2} methods on HFIB spheroids size. (a) Area measurements and (b) optical microscopy images of noncleared spheroids, spheroids cleared using Clear^{T2}/4, Clear^{T2}/8, or Clear^{T2}/10 methods, and spheroids after reversing the clearing process. Scale bars correspond to 200 μm. Data are presented as mean ± s.d. ($n = 8$), n.s. means nonsignificant.

3 Results and Discussion

In this study, spheroids composed of HFIB cells were chosen due to their superior capacity to maintain their structure and integrity during the clearing process, as previously demonstrated by our group.[10] Such approach bypasses interferences of spheroids' low cohesiveness on their structure and size during the clearing method.

Spheroids were produced by seeding cells on nonadhesive concave microwells, resulting in the formation of reproducible 3-D spherical cellular aggregates with a diameter of 396.17 ± 28.72 μm, after 6 days of culture. After spheroids' fixation, they were stained with PI, a red-fluorescent stain that has been widely used for the evaluation of spheroids cellular viability through fluorescence microscopy[10,33,34] and also in other works for optimizing the clearing methods.[35–37] Then, whole spheroids were cleared by immersing them in formamide/PEG solutions [MW: 4000 Da (Clear^{T2}/4), 8000 Da (Clear^{T2}/8), or 10,000 Da (Clear^{T2}/10)] and then they were observed through optical and CLSM.

3.1 Clear^{T2} *Clearings Do Not Influence Spheroids' Size and Enhance their Transparency*

A suitable clearing method must preserve samples' size and structure in order to allow the study of its initial morphology.[35] Additionally, the clearing method should not increase samples' dimensions, since larger samples require longer imaging times and they may also become unsuited for whole imaging through CLSM.[6] Therefore, the effect of Clear^{T2} methods in the preservation of the spheroids' morphology was evaluated by comparing the area of the cleared spheroids with that of the noncleared spheroids (Fig. 2).

The mean area of the spheroids cleared by Clear^{T2}/4, Clear^{T2}/8, and Clear^{T2}/10 increased by 10.35%, 9.91%, and 10.11%, respectively, when compared to that of the noncleared spheroids [Fig. 2(a)]. The slight increase of spheroids' size was not statistically significant, which demonstrates that all the Clear^{T2} methods did not induce any significant changes on the spheroids' morphology and that PEG MW does not affect spheroids' size during the clearing procedure (Fig. 2). Similar

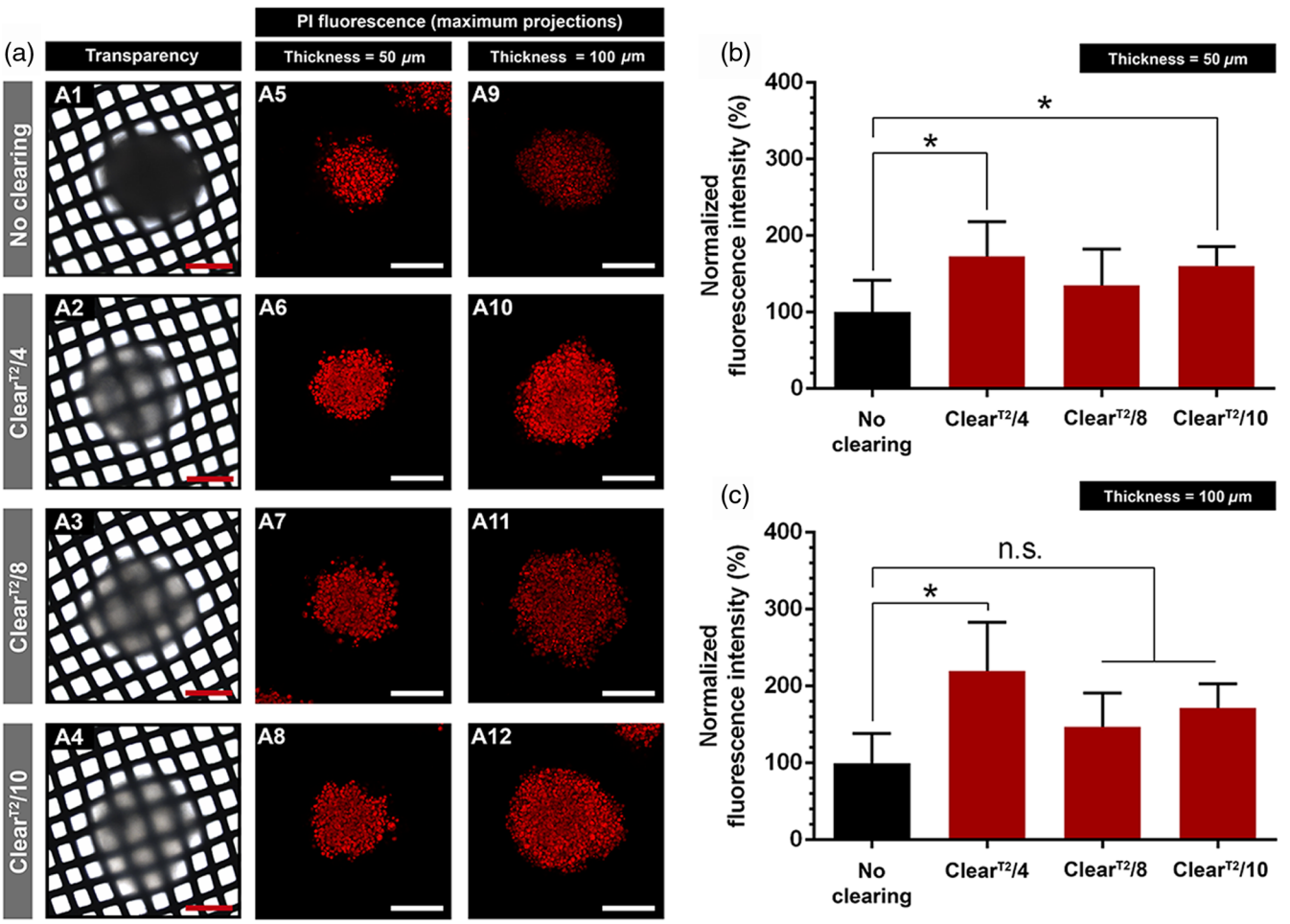

Fig. 3 Influence of Clear^{T2} methods on HFIB spheroids transparency and PI fluorescence intensity. (a1)–(a4) Optical transparency of noncleared spheroids and cleared spheroids with Clear^{T2}/4, Clear^{T2}/8, and Clear^{T2}/10. Spheroids were imaged on crosshatched backgrounds to show relative differences in transparency. (a5)–(a12) CLSM images of PI-stained noncleared and Clear^{T2}/4, Clear^{T2}/8, and Clear^{T2}/10 cleared spheroids. Each image is a maximum projection of the z-stacks (thickness: 50 and 100 μm). Analysis of the fluorescence intensity of the spheroids stained with PI for the maximum projections of (b) 50 and (c) 100 μm of thickness. Scale bars correspond to 200 μm. Data are presented as mean $\pm$ s.d. ($n = 5$), $^*p < 0.05$, and n.s. means nonsignificant.

results were obtained in other studies, which demonstrated that the Clear^{T2} method performed with PEG 8000 Da did not induce significant volume changes on brain sections [22] or on spheroids.[26] In fact, morphological and volumes changes are mostly associated with organic solvent-based clearing methods, which use benzylalcohol/benzylbenzoate (e.g., BABB) or dichloromethane/dibenzylether (e.g., 3DISCO and iDISCO).[6]

The capacity of the Clear^{T2} clearing methods to enhance the transparency of spheroids was also observed in the optical microscopy images, as previously reported in the literature.[21,22,26,35,36,41] The results demonstrated that, independently of the PEG MW used in the clearing process, all spheroids become gradually more transparent after each immersion step in the clearing solutions [Figs. 3(a1)–3(a4) and (9)]. In fact, the transparency of the spheroids did not seem to differ among the different Clear^{T2} methods variations. Such is explained by the fact that formamide is the main agent responsible for rendering transparency to the cells,[6,42] and that all the samples were immersed in solutions containing the same concentration of formamide.

3.2 Clear^{T2} *Clearing Methods Are Reversible*

The reversibility of the clearing methods, i.e., if the cleared samples can return to their original morphology and nontransparency, is also important for the application of spheroids in therapeutics screening.[22,23] According to Ke et al.,[23] the reversibility of the clearing method also enables the analysis of the same samples by other techniques (e.g., immunohistochemistry). Additionally, nonreversible clearing methods may be indicative that the sample is chemically modified during its treatment, leading to unrealistic interpretations.[23]

Kuwajima et al.[22] already demonstrated that the Clear^{T2} method that uses PEG 8000 Da can be reversed by immersing samples of mice embryos in PBS. Herein, it was evaluated if PEGs with other MW have any influence in the clearing reversal process of the spheroids. For this purpose, the size and transparency of the cleared spheroids were also evaluated after immersion in a PBS solution during 30 min. Independently of the Clear^{T2} method used, all spheroids maintained their original size [Fig. 2(a)] and were able to return to their nontransparent state (Fig. 9). Therefore, the results indicate that the PEG MW does not influence the Clear^{T2} reversibility and/or that it does not induce permanent modifications on spheroids' general structure.

3.3 Clear^{T2} *Methods Preserve the PI Fluorescence Intensity*

The clearing process should not affect negatively the fluorescence intensity of the samples, i.e., clearing methods must preserve the fluorescence intensity in order to allow their imaging through fluorescence microscopy. In previous studies, it was demonstrated that some clearing methods, such as BABB[43]

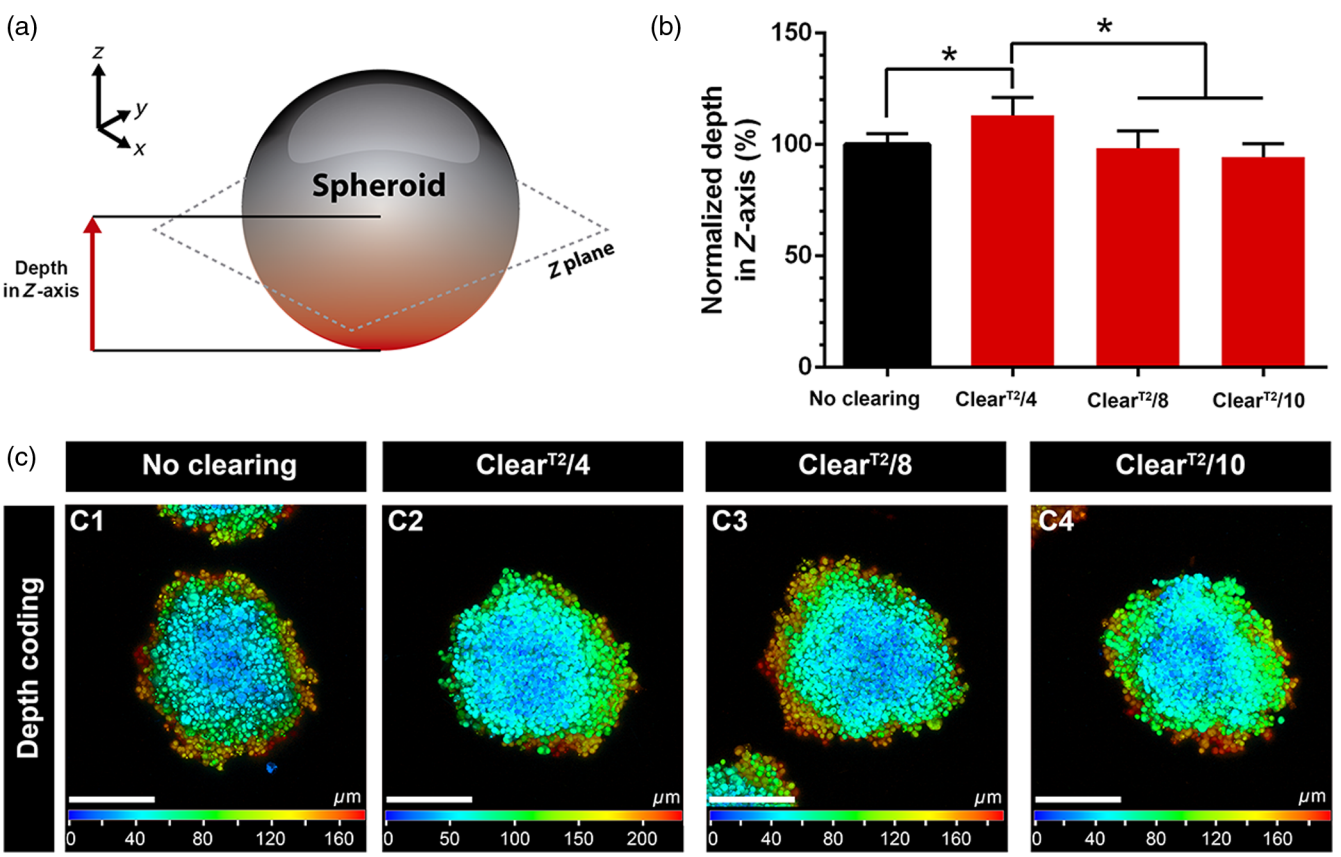

Fig. 4 Quantitative representation of PI imaging depth in the HFIB spheroids. (a) Schematic representation of the penetration depth measured in the spheroids. (b) Penetration depth of PI fluorescence signal and (c) depth coding CLSM images of (c1) noncleared, (c2) Clear^{T2}/4, (c3) Clear^{T2}/8, and (c4) Clear^{T2}/10 cleared spheroids. Scale bars correspond to 200 μm. Data are presented as mean $\pm$ s.d. ($n = 5$) and $^*p < 0.05$.

and Scale,[41] lack in the preservation of the probes fluorescence intensity due to the fluorescence quenching effect. Such effect was also observed in tissues that were only cleared with formamide (Clear^{T} method).[22] This result may be explained by protein denaturation caused by formamide.[6] To surpass this drawback, PEG was added to the formamide solutions to stabilize proteins' structure and maintain their fluorescence. Kuwajima et al.[22] reported that the addition of PEG 8000 Da to formamide resulted in the preservation of the fluorescence of proteins, immunohistochemistry labelings, and dye tracers (e.g., 1,1′-dioctadecyl-3,3,3′,3′-tetramethylindocarbocyanine perchlorate, cholera toxin subunit B). Still, in other studies, it was demonstrated that the use of PEG 8000 Da did not contribute to preserve the fluorescence intensity of PI within mice brain sections.[35]

Therefore, we investigated the influence of the PEG MW on the Clear^{T2} capacity to preserve the fluorescence intensity of labeled spheroids. For this purpose, the fluorescence of the PI-stained noncleared and Clear^{T2}/4, Clear^{T2}/8, and Clear^{T2}/10 cleared spheroids was determined as previously described elsewhere (see Appendix for further details).[35] From the analysis of the maximum projection images (thickness equal to 50 and 100 μm) [Figs. 3(a5)–3(a12)], it was possible to verify that all the Clear^{T2} methods under investigation were able to preserve the fluorescence of the PI [Figs. 3(b) and 3(c)]. However, among the Clear^{T2} methods variations, Clear^{T2}/4 demonstrated a significantly higher capacity to preserve the PI fluorescence, even at deep penetration depths [Figs. 3(b) and 3(c)]. Importantly, this improved fluorescence intensity was not prompted by the autofluorescence of the clearing solutions constituents, since all the solutions used in the various Clear^{T2} methods have a transmittance of ≈100% from 400 to 800 nm (the absorbance peaks of the PEG polymers-formamide solutions occur below 400 nm and according to literature PEG

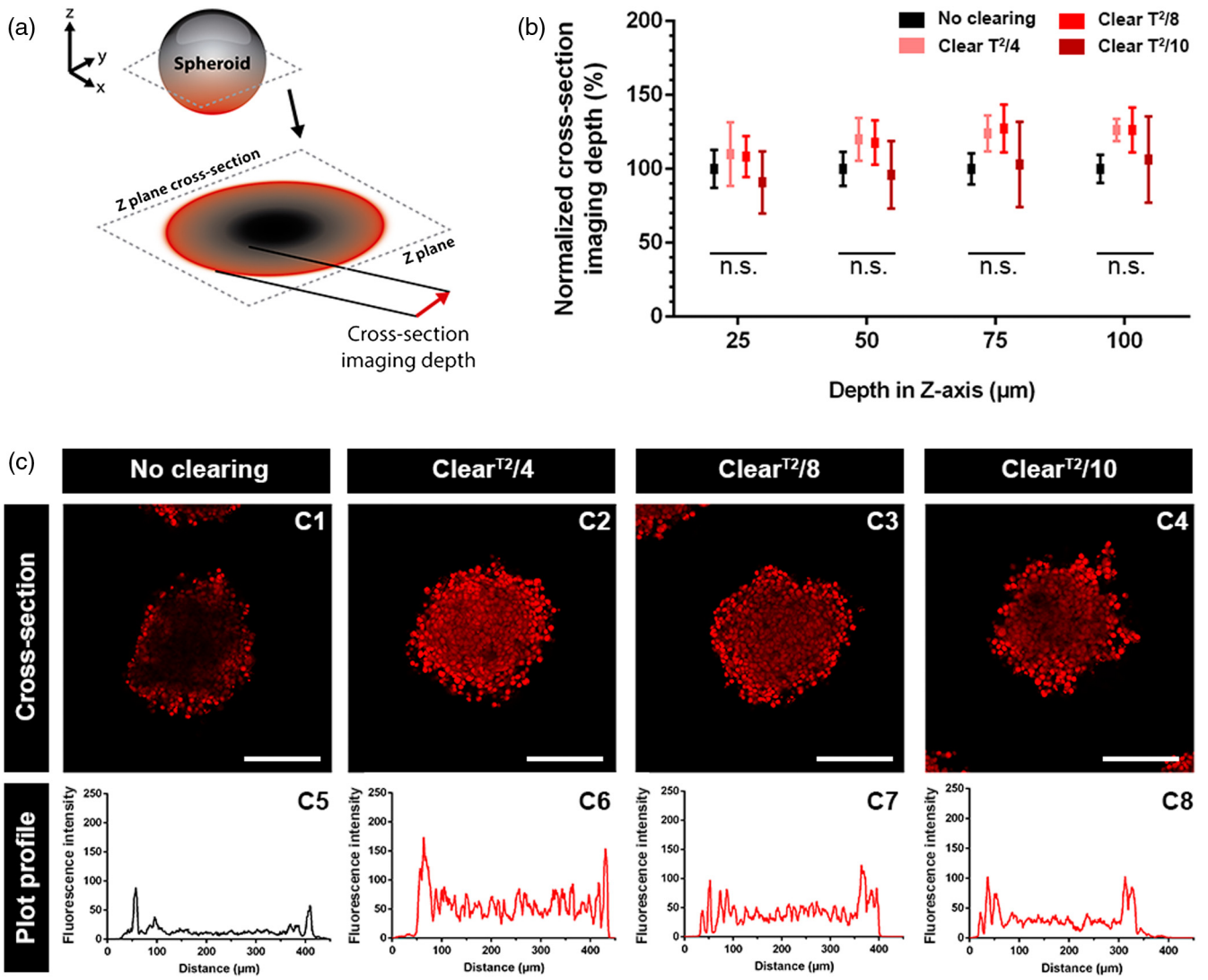

Fig. 5 HFIB spheroids PI cross-section imaging depth analysis. (a) Schematic illustration of the spheroids PI cross-section imaging depth measurements. (b) Spheroids PI cross-section imaging depth analysis. (c) Cross-section CLSM images of (c1) noncleared, (c2) Clear^{T2}/4, (c3) Clear^{T2}/8, and (c4) Clear^{T2}/10 cleared spheroids. Plot profiles of CLSM images of the (c5) noncleared, (c6) Clear^{T2}/4, (c7) Clear^{T2}/8, and (c8) Clear^{T2}/10 cleared spheroids. CLSM images correspond to a z-tack at a penetration depth of 75 μm. Scale bars correspond to 200 μm. Data are presented as mean ± s.d. ($n = 5$), n.s. means nonsignificant.

has absorbance below 400 nm[44,45]) (Fig. 10). In other words, the clearing solutions are permissive to the PI excitation laser light (514 nm), and the emitted fluorescence (550 to 750 nm) is not absorbed by the solutions (Fig. 10). Moreover, nonstained cleared spheroids did not present fluorescence signals when analyzed in the same conditions used for PI-stained spheroids (Fig. 11).

3.4 *PI Imaging Depth and Cross-Section Imaging Are Significantly Improved Using the* Clear^{T2}/4 *Method*

The fluorescence signal depth in CLSM is limited by the equipment (e.g., the working distance of the commonly used objectives) and also by the scattering phenomena between the specimen and the excitation and emission photons.[4,6] Consequently, CLSM is more prone to be used for the imaging of thin samples [e.g., two-dimensional (2-D) cultures or sliced tissues]. Nevertheless, to improve the imaging of whole thick samples (e.g., spheroids) by CLSM and avoid the handicaps associated with samples sectioning,[4,19,20] the reduction of the light scattering using optical clearing methods has been investigated.[16] To accomplish that, some clearing methods (e.g., Scale) remove the cellular lipids that are the main source of light scattering.[6,21] On the other hand, clearing methods, such as the Clear^{T2}, reduce the inhomogeneity of the light scatter by equilibrating the RI throughout the sample.[6] In the Clear^{T2} method, the formamide and PEG aqueous solutions have an RI $\approx$ 1.44 that will match with the overall RI of the fixed tissue (RI $\approx$ 1.50).[6,29,46]

To study the possible improvement in the imaging depth after spheroids clearing by Clear^{T2} methods and the PEG MW influence on this process, the penetration depth of the PI fluorescence signal was measured and presented in Fig. 4 (see Appendix for details). The results show that the Clear^{T2}/4 improved significantly the penetration depth of the PI signal [Figs. 4(b) and 4(c)]. In fact, the use of PEG 4000 Da allowed to detect PI signal up to 211.67 $\pm$ 16.81 μm, whereas the PEG 8000 and 10,000 Da only enabled the acquisition of a signal up to 183.89 $\pm$ 14.13 and 176.43 $\pm$ 11.44 μm, respectively.

The cross-section imaging depth was also analyzed to demonstrate the influence of the Clear^{T2} clearing method, as well as the PEG MW in the PI-stained spheroids observation by CLSM (see Appendix for details). This evaluation was performed to determine which method is more suitable for acquiring fluorescence from the interior of the spheroid. In comparison to the noncleared spheroids, spheroids cleared with Clear^{T2} methods allowed the acquisition of images from PI-stained cells that were in the interior of the spheroid (Fig. 5), such is even more evident at the penetration depth of 100 μm [Fig. 5(b)].

At this penetration depth, the spheroids fluorescence signal in the cross-section improved 24.95% $\pm$ 7.50%, 24.95% $\pm$ 15.07%, and 6.31% $\pm$ 29.11% when cleared with Clear^{T2}/4, Clear^{T2}/8, and Clear^{T2}/10, respectively. To corroborate these observations, plot profiles of the noncleared and cleared spheroids CLSM cross-section images at 75 μm of penetration depth (Z-axis) were performed [Fig. 5(c)] (see Appendix for details). These graphs display the color intensity of the pixels throughout the spheroid cross section. As observed in Figs. 5(c1)–5(c4), without the use of a clearing method, the fluorescence observed within spheroids' core is limited. On the other side, the Clear^{T2}/4 clearing method allowed a better observation of the spheroid's interior and also the attainment of a higher PI fluorescence intensity, when compared to the other Clear^{T2} methods variations [Figs. 5(c5)–5(c8)].

This improved imaging capacity of the Clear^{T2}/4 method may be linked to the smaller size of the polymer chain of PEG 4000. Such may facilitate the PEG distribution and penetration throughout the spheroid and, consequently, the stabilization of the fluorescence probe in deeper regions, thus allowing a better imaging. In fact, large molecules penetrate slowly into the tissues[47] and lower MWs are generally associated with higher diffusion coefficients.[48] Moreover, the use of PEG with a low MW may further contribute to a quicker establishment of the water balance between the clearing solution and the spheroids, leading to an improved penetration of the clearing agent through the spheroid caused by the osmotic pressure.[49–52] In future works, it may be interesting to use PEG with smaller MW (e.g., PEG 400 Da) to assess if they further improve the clearing efficacy of the Clear^{T2} method.

4 Conclusions

Clearing methods have been used to allow the observation and analysis of thick tissue samples and more recently spheroids by fluorescence microscopy, such as CLSM. In this work, we investigated for the first time the influence of PEG MW on Clear^{T2} clearing method ability to improve the imaging of PI-stained HFIB spheroids. In general, all the Clear^{T2} methods variations (Clear^{T2}/4, Clear^{T2}/8, and Clear^{T2}/10) allowed to obtain transparent spheroids without influencing their original size. Compared to the other Clear^{T2} methods, the Clear^{T2}/4 improved the imaging of the spheroids in what concerns (i) fluorescence intensity preservation, (ii) penetration depth, and (iii) cross-section imaging depth. Such improvements allow us to conclude that the use of PEG 4000 Da can be an improved alternative to the conventional Clear^{T2}/8 methodology for the imaging of thick samples through fluorescence microscopy techniques, namely in the observation of the spheroids' necrotic core or the cellular death induced by a therapeutic molecule using PI fluorescent staining. Ultimately, this article may contribute to the translation of analytical techniques, commonly used for in 2-D cell cultures, to 3-D cell cultures and, therefore, support the application of these models in the pharmaceutical industry.

Appendix

A.1 Spheroids Optical Microscopy and CLSM Images Analysis

All the analyses described hereafter were performed using an image processing program designed for scientific analysis—ImageJ, National Institutes of Health.[40]

A.1.1 *Measurement of the spheroids area and transparency*

Spheroids area before and after the clearing process, and after clearing reversal was determined by analyzing optical microscopy images (Olympus CX41 inverted optical microscope equipped with an Olympus SP-500 UZ digital camera), as previously demonstrated in our work.[10] In brief, the area of spheroids was selected in the image using a threshold and then the area of the spheroids was determined by converting the area in pixels to μm^2 values (Fig. 6).

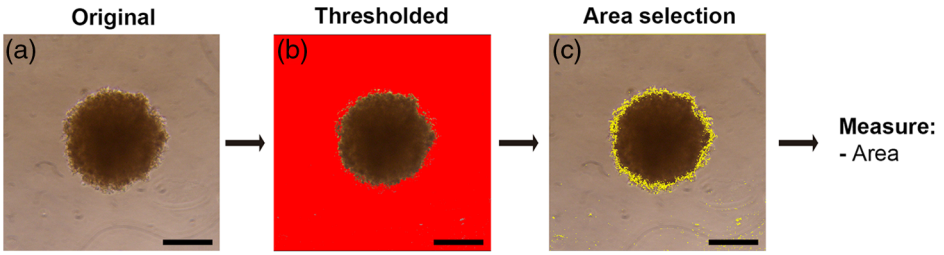

Fig. 6 Schematic representation of the procedures used for the measurement of the spheroids area through optical microscopic images. Scale bars correspond to 200 μm.

The transparency of the spheroids before and after clearing, as well as after the clearing reversal, was observed by placing the spheroids on a grill that will serve as a crosshatched background to show relative differences in transparency (as performed previously[21,22,26,35,36,41]). Then, optical microscopy images were acquired using a Carl Zeiss Axio Imager A1 inverted microscope equipped with an AxioVision camera.

A.1.2 *Measurement of PI fluorescence intensity*

The determination of the PI fluorescence levels in the spheroids was performed as previously described by Yu et al.[35] and Grist and Nasseri.[53] Initially, a maximum intensity z-projection of the CLSM image with a thickness of 50 and 100 μm (10 and 20 z-stacks, respectively) was performed [Fig. 7(a)]. Then, the spheroid area was selected by applying a threshold [Figs. 7(b) and 7(c)]. Afterward, the integrated density (ID), the selected area (A), and the mean fluorescence of the background (MFB) (region without fluorescence) were measured. These values were then used to determine the PI fluorescence intensity through the calculation of the corrected total cell fluorescence (CTCF)[54]

$$\mathrm{CTCF} = \mathrm{ID} - (A \times \mathrm{MFB}), \tag{1}$$

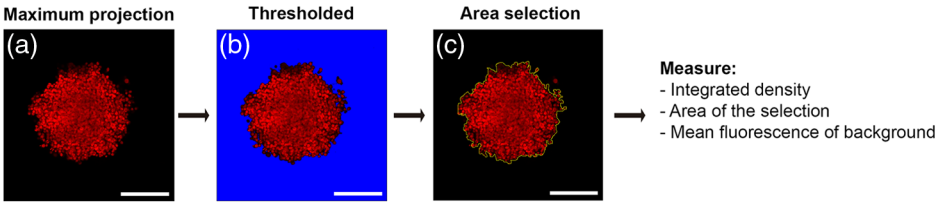

Fig. 7 Schematic representation of the procedures used in the analysis of CLSM images to evaluate the spheroids PI fluorescence intensity by calculating the CTCF. Scale bars correspond to 200 μm.

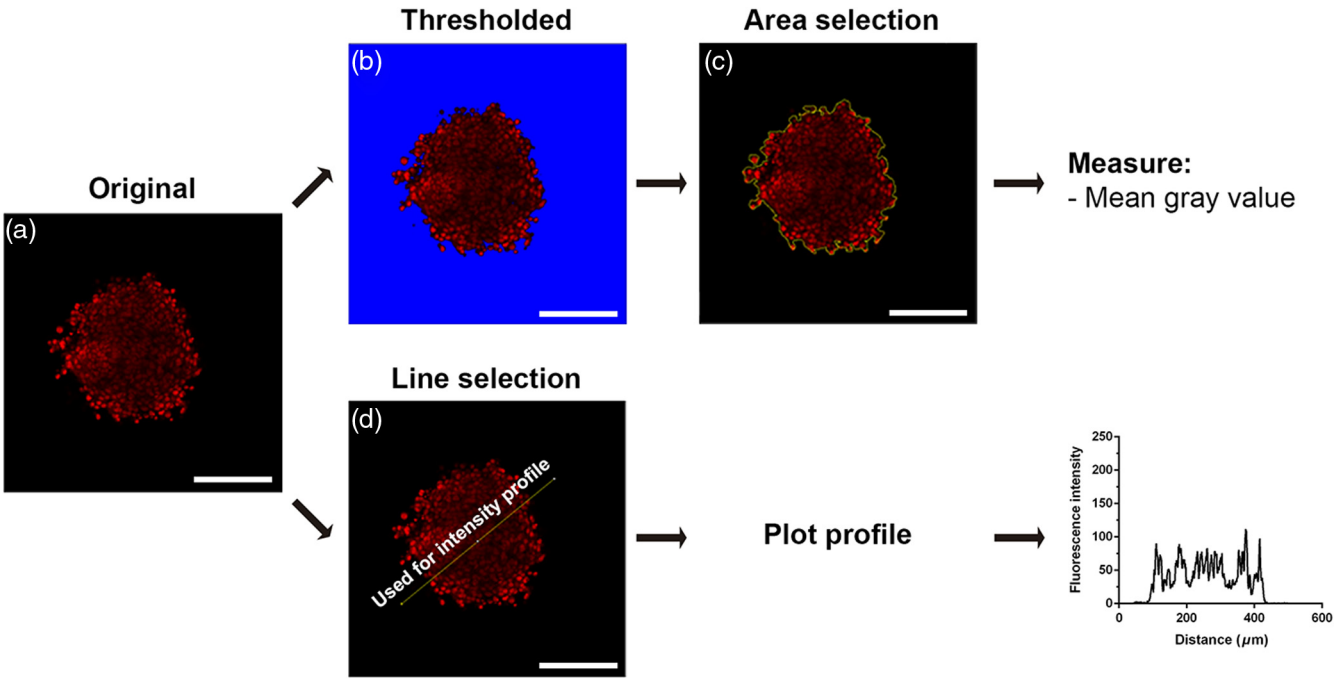

Fig. 8 Schematic representation of the procedures used to analyze the PI cross-section imaging depth by the determination of mean gray value and plot profile. Scale bars correspond to 200 μm.

where the variable ID, A, and MFB correspond to integrated density, area of the selection, and mean fluorescence of the background, respectively.

A.1.3 *Measurement of the PI imaging depth and cross-section imaging depth*

The imaging depth of PI was determined by multiplying the number of stacks with PI fluorescence signal by the z-stacks thickness (5 μm).

The determination of the PI cross-section imaging depth was performed by calculating the mean gray value of the spheroid selected area at 25, 50, 75 and 100 μm of penetration depth (Fig. 8). The mean gray value is a relation between the number of pixels with color in a selected area and the intensity of this color. When the mean gray value is equal to 0, it corresponds to pixels without color (no fluorescence). Mean gray values between 1 and 250 correspond to pixels with color and higher mean gray value corresponds to higher color intensity.

Additionally, similarly to previous works,[41,55] the cross-section imaging depth of PI in the spheroids was analyzed by tracing plot profiles, i.e., a graph of the pixels fluorescence intensities along a line traced in the spheroid [Fig. 8(d)]. The plot profiles were obtained at 75 μm of penetration depth. Lastly, the spheroids transparency (Fig. 9), optical clearing solutions absorbance and transmittance (Fig. 10) and the autofluorescence of cleared nonstained spheroids (Fig. 11) were analyzed.

Disclosures

The authors declare no financial or commercial conflicts of interest.

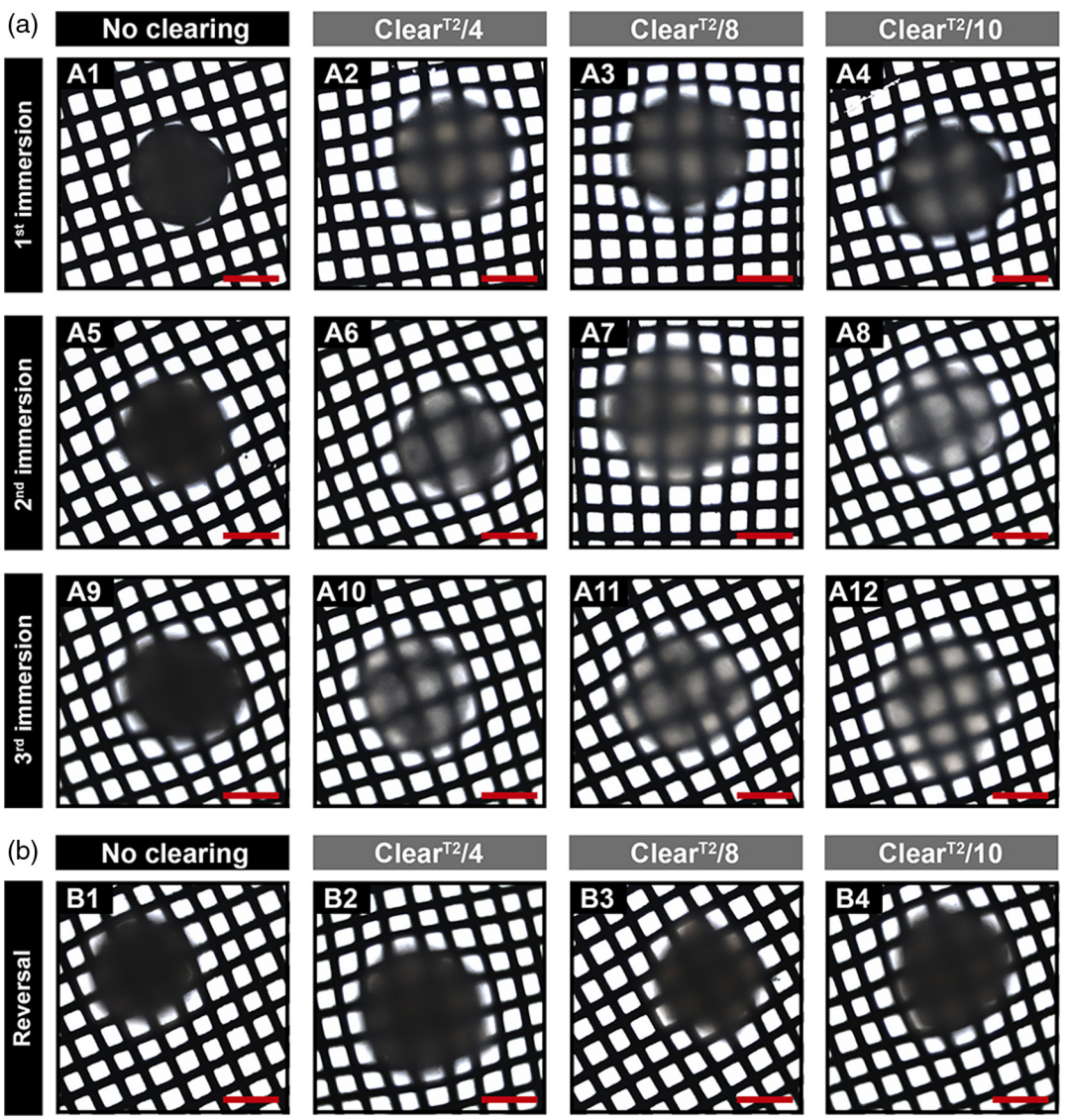

Fig. 9 HFIB spheroids transparency after the Clear^{T2} methods. (a) Optical transparency of noncleared spheroids and cleared spheroids with Clear^{T2}/4, Clear^{T2}/8, and Clear^{T2}/10. (b) Spheroids transparency after clearing reversal with PBS for 30 min. Spheroids were imaged on crosshatched backgrounds to show relative differences in transparency. Scale bars correspond to 200 μm.

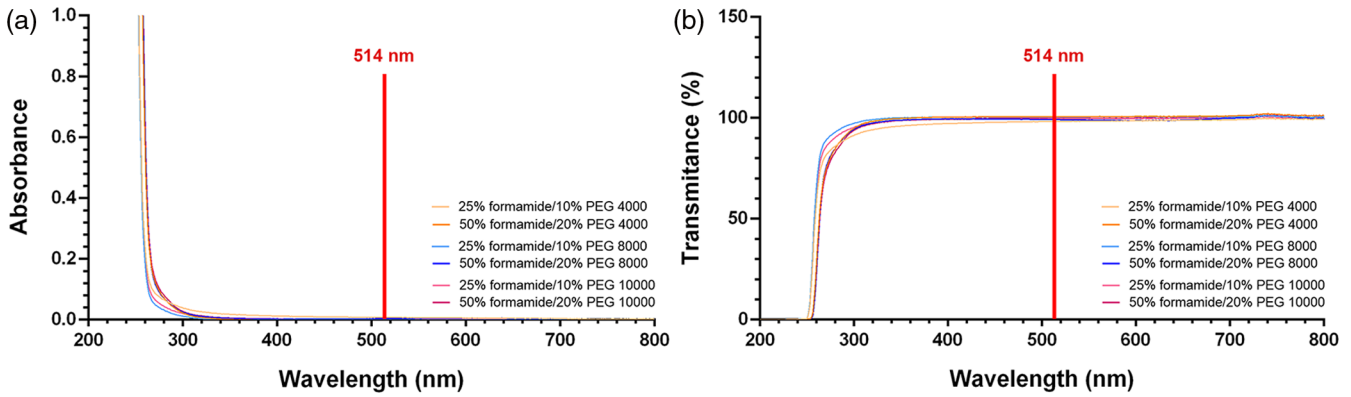

Fig. 10 (a) Absorbance and (b) transmittance of the solutions used on the Clear^{T2}/4, Clear^{T2}/8, and Clear^{T2}/10 clearing methods.

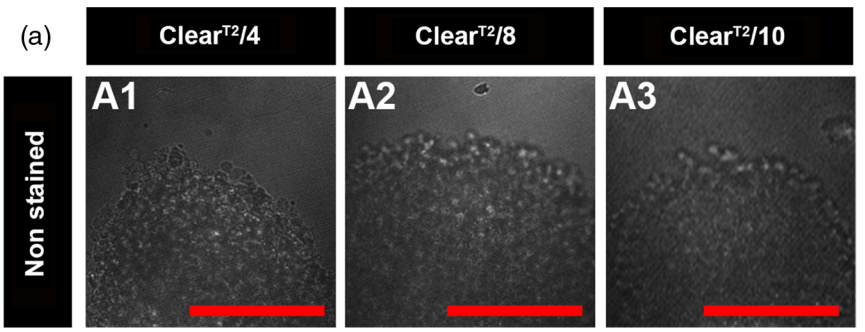

Fig. 11 Autofluorescence of cleared nonstained spheroids. Differential interference contrast merged with fluorescence images (red channel) of nonstained (b1) Clear^{T2}/4, (b2) Clear^{T2}/8, and (b3) Clear^{T2}/10 cleared spheroids. Images correspond to a *z*-stack at a penetration depth of 25 μm Scale bars correspond to 200 μm.

Acknowledgments

This work was supported by the FEDER funds through the POCI - COMPETE 2020 - Operational Programme Competitiveness and Internationalisation in Axis I - Strengthening research, technological development, and innovation (Project POCI-01-0145-FEDER-007491) and the National Funds by FCT - Foundation for Science and Technology (Project UID/Multi/00709/2013). André F. Moreira, Duarte de Melo-Diogo, and Elisabete C. Costa acknowledge for their Grants: SFRH/BD/109482/2015, SFRH/BD/103506/2014, and SFRH/BD/103507/2014, respectively. The funders had no role in the decision to publish or in the preparation of the paper.

References

1. E. Fennema et al., "Spheroid culture as a tool for creating 3D complex tissues," *Trends Biotechnol.* **31**(2), 108–115 (2013).
2. T.-M. Achilli, J. Meyer, and J. R. Morgan, "Advances in the formation, use and understanding of multi-cellular spheroids," *Expert Opin. Biol. Ther.* **12**(10), 1347–1360 (2012).
3. S. Breslin and L. O'Driscoll, "Three-dimensional cell culture: the missing link in drug discovery," *Drug Discovery Today* **18**(5–6), 240–249 (2013).
4. E. C. Costa et al., "3D tumor spheroids: an overview on the tools and techniques used for their analysis," *Biotechnol. Adv.* **34**(8), 1427–1441 (2016).
5. G. Mehta et al., "Opportunities and challenges for use of tumor spheroids as models to test drug delivery and efficacy," *J. Controlled Release* **164**(2), 192–204 (2012).
6. D. S. Richardson and J. W. Lichtman, "Clarifying tissue clearing," *Cell* **162**(2), 246–257 (2015).
7. I. Smyrek and E. H. K. Stelzer, "Quantitative three-dimensional evaluation of immunofluorescence staining for large whole mount spheroids with light sheet microscopy," *Biomed. Opt. Express* **8**(2), 484–499 (2017).
8. X. Gong et al., "Generation of multicellular tumor spheroids with microwell-based agarose scaffolds for drug testing," *PLoS One* **10**(6), e0130348 (2015).
9. O. Sirenko et al., "High-content assays for characterizing the viability and morphology of 3D cancer spheroid cultures," *ASSAY Drug Dev. Technol.* **13**(7), 402–414 (2015).
10. E. C. Costa et al., "Optimization of liquid overlay technique to formulate heterogenic 3D co-cultures models," *Biotechnol. Bioeng.* **111**(8), 1672–1685 (2014).
11. M. P. Carvalho, E. C. Costa, and I. J. Correia, "Assembly of breast cancer heterotypic spheroids on hyaluronic acid coated surfaces," *Biotechnol. Prog.* **33**(5), 1346–1357 (2017).
12. S. Camões et al., "Human neonatal mesenchymal stem cell spheroids-conditioned medium accelerates skin regeneration," *Toxicol. Lett.* **238**(2), S376–S377 (2015).
13. V. M. Gaspar et al., "Folate-targeted multifunctional amino acid-chitosan nanoparticles for improved cancer therapy," *Pharm. Res.* **32**, 562–577 (2014).
14. A. F. Moreira et al., "Thermo- and pH-responsive nano-in-micro particles for combinatorial drug delivery to cancer cells," *Eur. J. Pharm. Sci.* **104**, 42–51 (2017).
15. S.-Y. Jeong et al., "Co-culture of tumor spheroids and fibroblasts in a collagen matrix-incorporated microfluidic chip mimics reciprocal activation in solid tumor microenvironment," *PLoS One* **11**(7), e0159013 (2016).

16. K. Svoboda and R. Yasuda, "Principles of two-photon excitation microscopy and its applications to neuroscience," *Neuron* **50**(6), 823–839 (2006).
17. X. Zhang et al., "Induction of mitochondrial dysfunction as a strategy for targeting tumour cells in metabolically compromised microenvironments," *Nat. Commun.* **5**, 3295 (2014).
18. S.-E. Yeon et al., "Application of concave microwells to pancreatic tumor spheroids enabling anticancer drug evaluation in a clinically relevant drug resistance model," *PLoS One* **8**(9), e73345 (2013).
19. F. Langenbach et al., "Generation and differentiation of microtissues from multipotent precursor cells for use in tissue engineering," *Nat. Protoc.* **6**(11), 1726–1735 (2011).
20. P.-A. Vidi, M. J. Bissell, and S. A. Lelièvre, "Three-dimensional culture of human breast epithelial cells: the how and the why," in *Epithelial Cell Culture Protocols*, S. H. Randell and L. M. Fulcher, Eds., pp. 193–219, Humana Press, Totowa, New Jersey (2013).
21. H. Hama et al., "Scale: a chemical approach for fluorescence imaging and reconstruction of transparent mouse brain," *Nat. Neurosci.* **14**(11), 1481–1488 (2011).
22. T. Kuwajima et al., "Clear^{T}: a detergent- and solvent-free clearing method for neuronal and non-neuronal tissue," *Development* **140**(6), 1364–1368 (2013).
23. M.-T. Ke, S. Fujimoto, and T. Imai, "SeeDB: a simple and morphology-preserving optical clearing agent for neuronal circuit reconstruction," *Nat. Neurosci.* **16**(8), 1154–1161 (2013).
24. L. Decroix et al., "Tissue clearing for confocal imaging of native and bio-artificial skeletal muscle," *Biotech. Histochem.* **90**(6), 424–431 (2015).
25. A. Azaripour et al., "A survey of clearing techniques for 3D imaging of tissues with special reference to connective tissue," *Prog. Histochem. Cytochem.* **51**(2), 9–23 (2016).
26. M. E. Boutin and D. Hoffman-Kim, "Application and assessment of optical clearing methods for imaging of tissue-engineered neural stem cell spheres," *Tissue Eng. Part C* **21**(3), 292–302 (2015).
27. Y. Y. Chen et al., "Clarifying intact 3D tissues on a microfluidic chip for high-throughput structural analysis," *Proc. Natl. Acad. Sci. U. S. A.* **113**(52), 14915–14920 (2016).
28. K. Tainaka et al., "Chemical principles in tissue clearing and staining protocols for whole-body cell profiling," *Annu. Rev. Cell Dev. Biol.* **32**, 713–741 (2016).
29. J. Seo, M. Choe, and S. Y. Kim, "Clearing and labeling techniques for large-scale biological tissues," *Mol. Cells* **39**(6), 439–446 (2016).
30. A. Feuchtinger, A. Walch, and M. Dobosz, "Deep tissue imaging: a review from a preclinical cancer research perspective," *Histochem. Cell Biol.* **146**(6), 781–806 (2016).
31. J. Morgenstern et al., "Effect of PEG molecular weight and PEGylation degree on the physical stability of PEGylated lysozyme," *Int. J. Pharm.* **519**(1), 408–417 (2017).
32. B. Treetharnmathurot et al., "Effect of PEG molecular weight and linking chemistry on the biological activity and thermal stability of PEGylated trypsin," *Int. J. Pharm.* **357**(1), 252–259 (2008).
33. S. Kessel et al., "Real-time viability and apoptosis kinetic detection method of 3D multicellular tumor spheroids using the Celigo image cytometer," *Cytometry A* **91**(9), 883–892 (2017).
34. B. Galateanu et al., "Impact of multicellular tumor spheroids as an in vivo-like tumor model on anticancer drug response," *Int. J. Oncol.* **48**(6), 2295–2302 (2016).
35. T. Yu et al., "Rapid and prodium iodide-compatible optical clearing method for brain tissue based on sugar/sugar-alcohol," *J. Biomed. Opt.* **21**(8), 081203 (2016).
36. J. R. Epp et al., "Optimization of clarity for clearing whole-brain and other intact organs," *eNeuro* **2**(3), ENEURO.0022-15.2015 (2015).
37. M. Fretaud et al., "High-resolution 3D imaging of whole organ after clearing: taking a new look at the zebrafish testis," *Sci. Rep.* **7**, 43012 (2017).
38. A. P. Napolitano et al., "Scaffold-free three-dimensional cell culture utilizing micromolded nonadhesive hydrogels," *Biotechniques* **43**(4), 494–500 (2007).
39. M.-T. Ke, S. Fujimoto, and T. Imai, "Optical clearing using SeeDB," *Bio-protocol* **4**(3), e1042 (2014).
40. W. S. Rasband, "ImageJ," 2008, http://rsbweb.nih.gov/ij/ (1 February 2018).
41. D. Kurihara et al., "ClearSee: a rapid optical clearing reagent for whole-plant fluorescence imaging," *Development* **142**(23), 4168–4179 (2015).
42. T. Yu et al., "RTF: a rapid and versatile tissue optical clearing method," *Sci. Rep.* **8**(1), 1964 (2018).
43. D. A. Yushchenko and C. Schultz, "Geklärte Gewebeproben für die optische Anatomie," *Angew. Chem.* **125**(42), 11151–11154 (2013).
44. A. Lasagni et al., "Rapid fabrication of biocompatible hydrogels micro-devices using laser interference lithography," *Proc. SPIE* **7365**, 73650I (2009).
45. T. Jayaramudu et al., "Preparation and characterization of poly(ethylene glycol) stabilized nano silver particles by a mechanochemical assisted ball mill process," *J. Appl. Polym. Sci.* **133**(7), 43027 (2016).
46. B. Hou et al., "Scalable and Dil-compatible optical clearance of the mammalian brain," *Front. Neuroanat.* **9**, 19 (2015).
47. J. A. Kiernan, "Formaldehyde, formalin, paraformaldehyde and glutaraldehyde: what they are and what they do," *Microsc. Today* **8**(1), 8–12 (2000).
48. D. Zhu et al., "Recent progress in tissue optical clearing," *Laser Photonics Rev.* **7**(5), 732–757 (2013).
49. L. Oliveira et al., "Optical clearing mechanisms characterization in muscle," *J. Innovative Opt. Health Sci.* **9**(5), 1650035 (2016).
50. V. V. Tuchin et al., "Light propagation in tissues with controlled optical properties," *J. Biomed. Opt.* **2**(4), 401–418 (1997).
51. I. Carneiro et al., "Water content and scatterers dispersion evaluation in colorectal tissues," *J. Biomed. Photonics Eng.* **3**(4), 040301 (2017).
52. I. Carneiro et al., "Simple multimodal optical technique for evaluation of free/bound water and dispersion of human liver tissue," *J. Biomed. Opt.* **22**(12), 125002 (2017).
53. S. M. Grist and S. S. Nasseri, "On-chip clearing of arrays of 3-D cell cultures and micro-tissues," *Biomicrofluidics* **10**(4), 044107 (2016).
54. P. Klaka et al., "A novel organotypic 3D sweat gland model with physiological functionality," *PLoS One* **12**(8), e0182752 (2017).
55. A. Masson et al., "High-resolution in-depth imaging of optically cleared thick samples using an adaptive SPIM," *Sci. Rep.* **5**, 16898 (2015).

Biographies for the authors are not available.